Supporting Information

An Integrated Self-healing Anode Assembled via Dynamic Encapsulation of Liquid Metal with 3D $Ti_3C_2T_x$ Network for Enhanced Lithium Storage

Hanning Zhang[1], Pengyu Chen[1], Huan Xia[1], Gang Xu[1], Yaping Wang[1], Tengfei Zhang[2*], Wenwen Sun[1], Muhammadali Turgunov[3], Wei Zhang[1*], ZhengMing Sun[1*]

[1]Jiangsu Key Laboratory of Advanced Metallic Materials, School of Materials Science and Engineering, Southeast University, Nanjing, 211189, China.
[2] College of Materials Science and Technology, Nanjing University of Aeronautics and Astronautics, Nanjing, 210016, China
[3] Department of Mechanical and Aerospace Engineering, Turin Polytechnic University, Tashkent 100095, Uzbekistan
*Corresponding authors: w69zhang@seu.edu.cn; zhangtengfei@nuaa.edu.cn; zmsun@seu.edu.cn

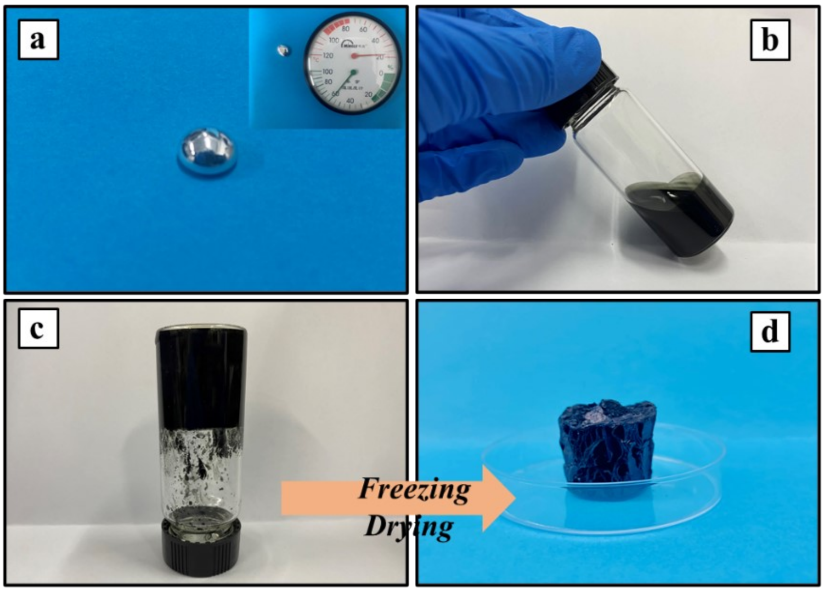

Figure S1 Photo image of colloid suspension of $Ti_3C_2T_x$ (a), bulk liquid metal (EGaIn-LM) at room temperature(b), LM-$Ti_3C_2T_x$ hydrogel precursor (c) and LM-$Ti_3C_2T_x$ foam (b).

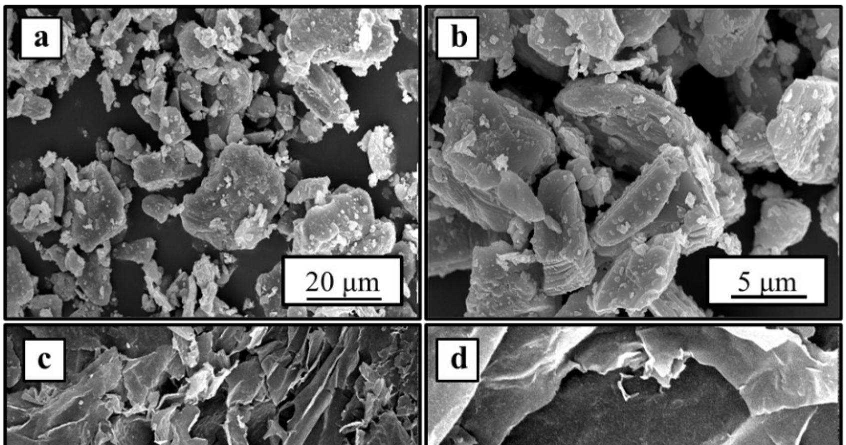

Figure S2 SEM image of Ti_3AlC_2 (a, b) and $Ti_3C_2T_x$ monolith (c, d) with different magnification.

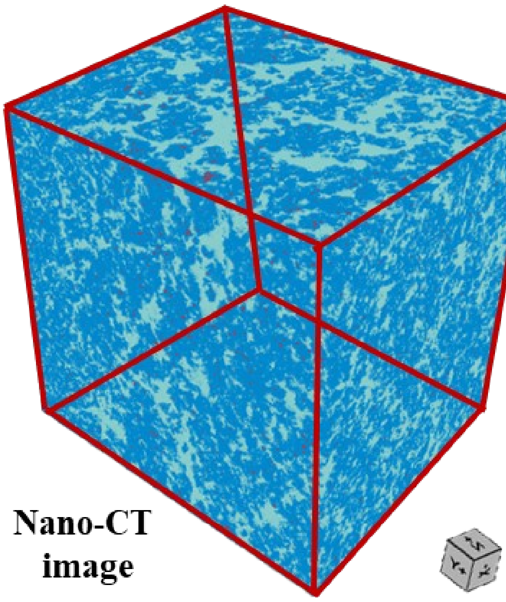

Figure S3 Nano-CT of LM-$Ti_3C_2T_x$

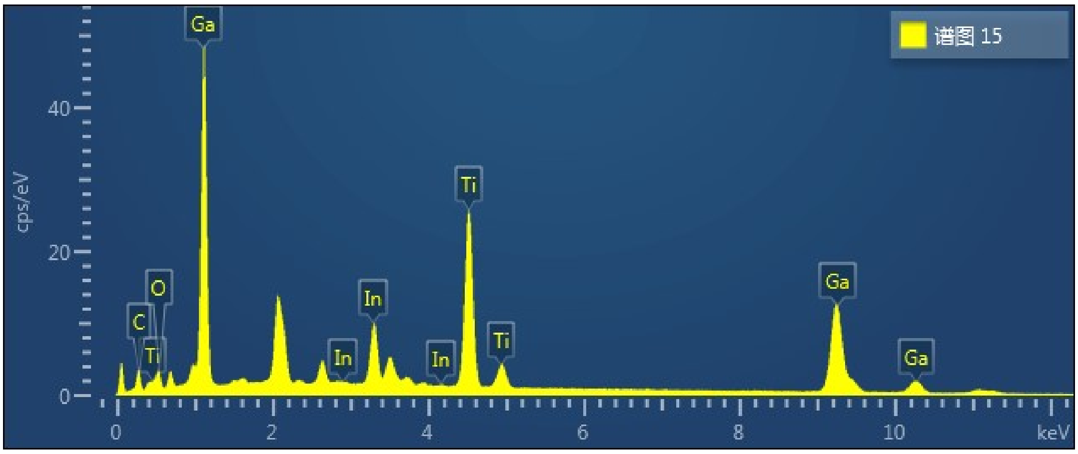

Element	wt%	Atom%
C	10.38	34.03
O	6.56	16.15
Ti	20.62	16.96
Ga	51.59	29.14
In	10.84	3.72
Total:	100.00	100.00

Figure S4 EDX of LM-$Ti_3C_2T_x$-2:1and corresponding element ratio.

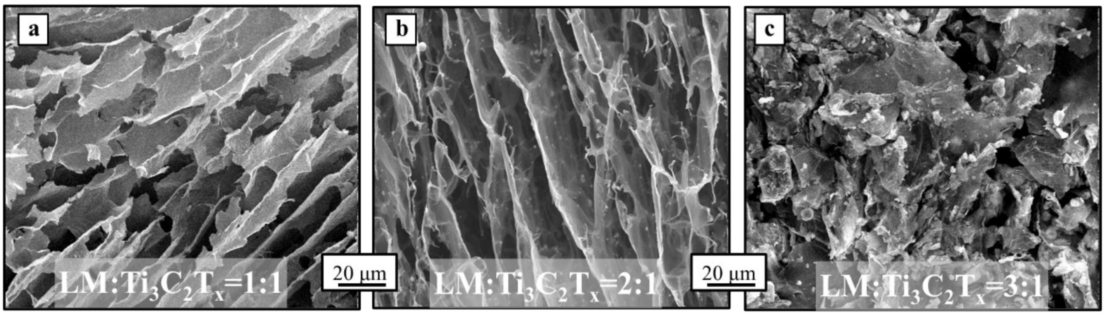

Figure S5 SEM images of LM-$Ti_3C_2T_x$ with different mass ratio.

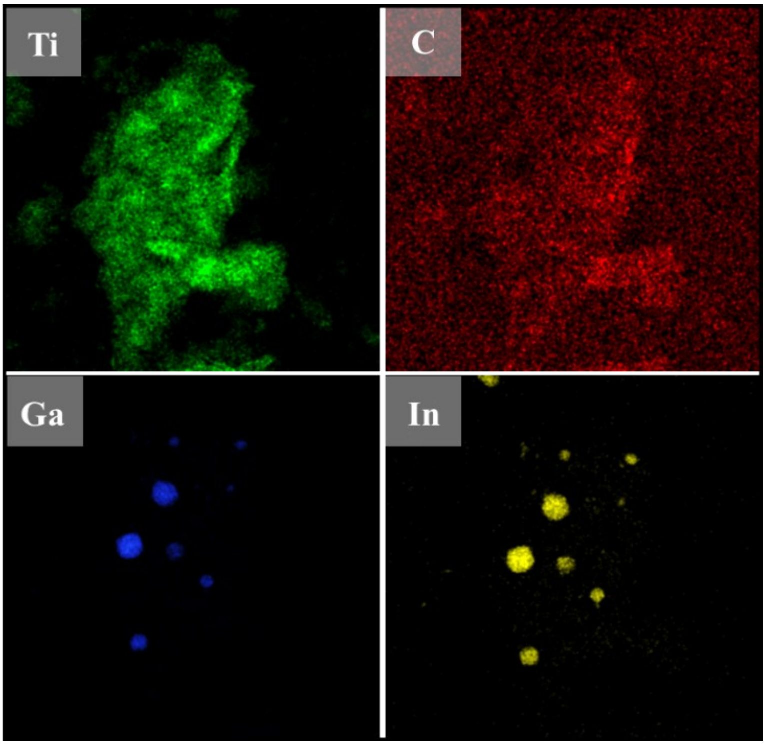

Figure S6 TEM Element distribution of LM-$Ti_3C_2T_x$

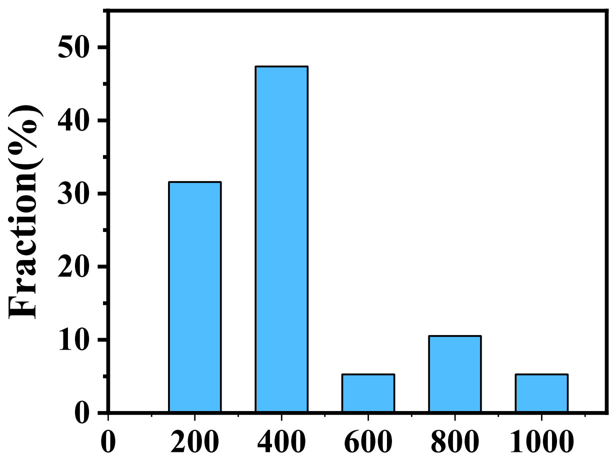

Figure S7 Average size diameter of LM-$Ti_3C_2T_x$, which is calculated to be 499.7 nm

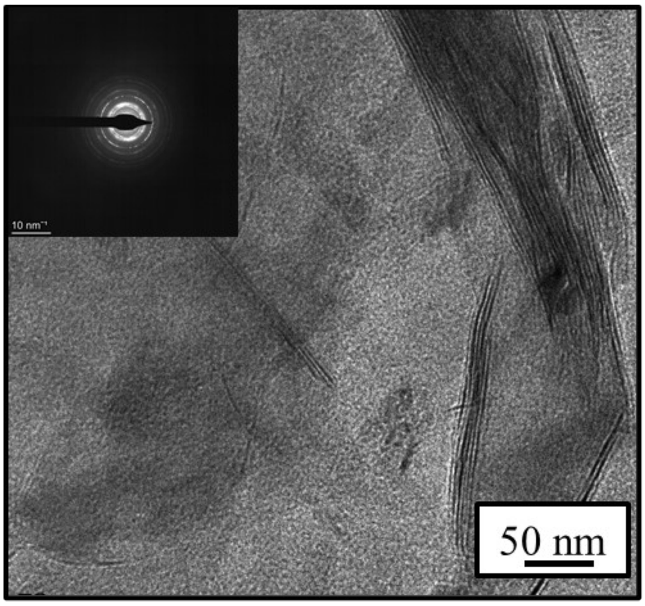

Figure S8 HRTEM and Selected area electron diffraction of LM-$Ti_3C_2T_x$

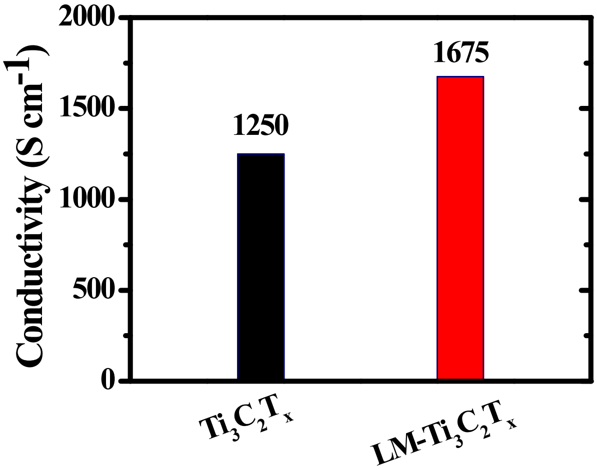

Figure S9 Conductivity of $Ti_3C_2T_x$ monolith and LM-$Ti_3C_2T_x$

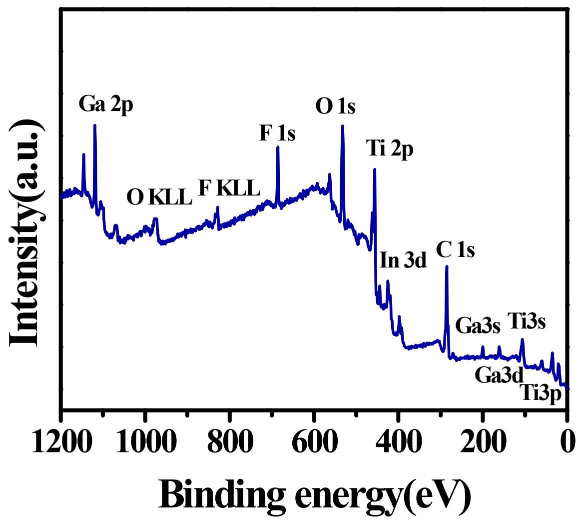

Figure S10 XPS full spectrum of LM-$Ti_3C_2T_x$

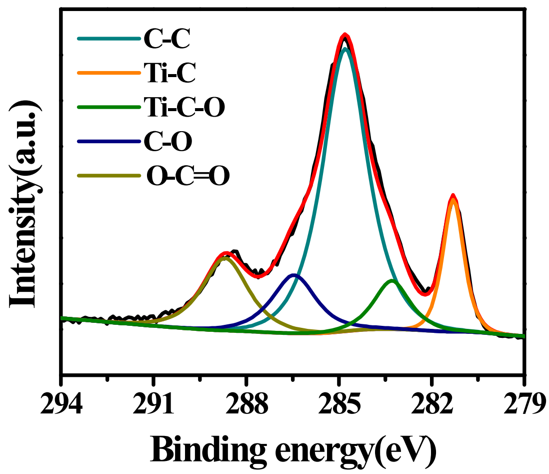

Figure S11 C 1s spectrum of LM-$Ti_3C_2T_x$

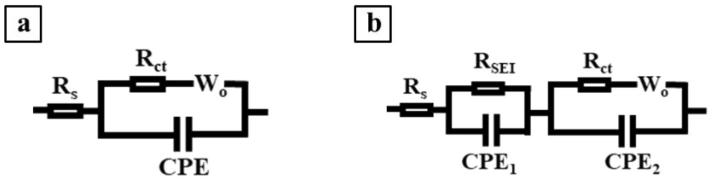

Figure S12 (a) Fitting the equivalent circuit diagram of LM-$Ti_3C_2T_x$ anode before and (b) after cycle

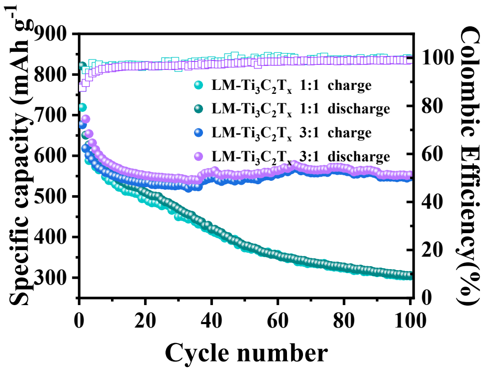

Figure S13 Cycling performance of LM-$Ti_3C_2T_x$ with different mass ratios at 0.1 A g^{-1} current density.

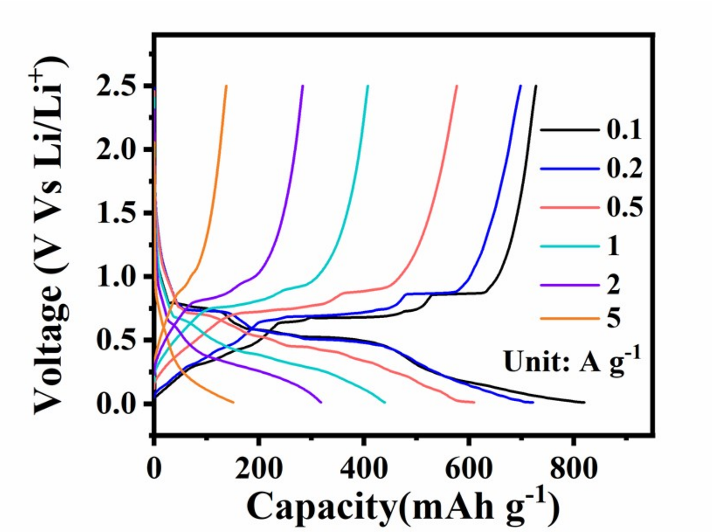

Figure S14 Galvanostatic charge/discharge curves of LMNPs, with an initial capacity of 819 mAh g^{-1}

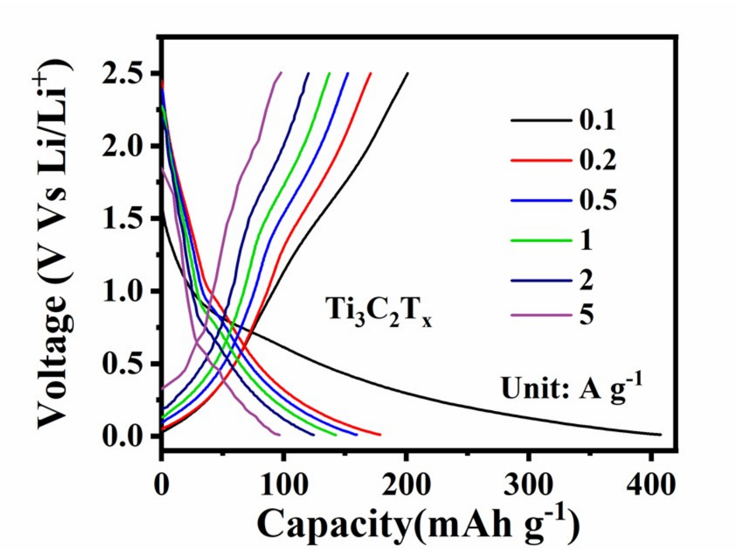

Figure S15 Galvanostatic charge/discharge curves of $Ti_3C_2T_x$ monolith, which show an initial capacity of 407 mAh g^{-1}, Since the mass content of $Ti_3C_2T_x$ is 37.3 wt.%, the capacity contribution is calculated to be 151.8 mAh g^{-1}. The calculation method is consistent with the relevant reports. [1]

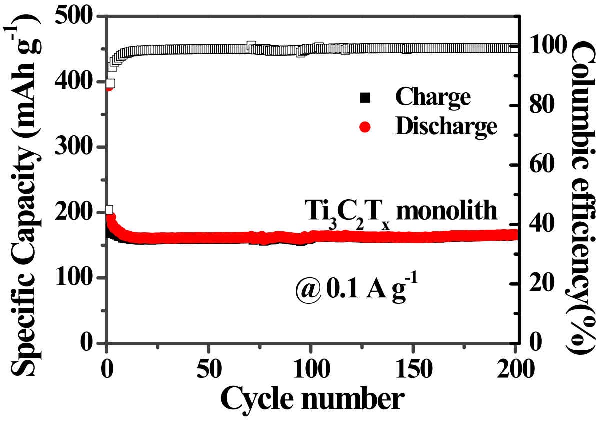

Figure S16 cycling performance of $Ti_3C_2T_x$ monolith at 0.1 A g^{-1}

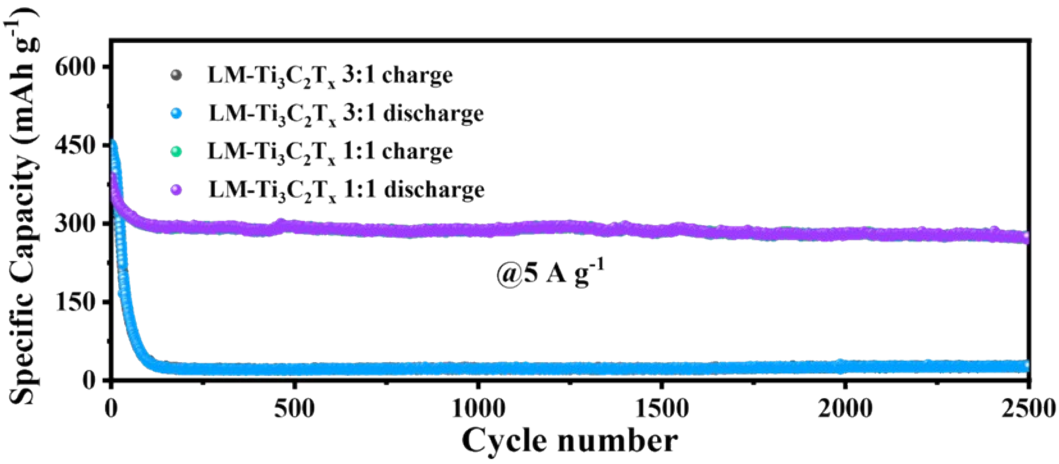

Figure S17 Cycling performance at 5 A g^{-1} of LM-$Ti_3C_2T_x$ with different mass ratio.

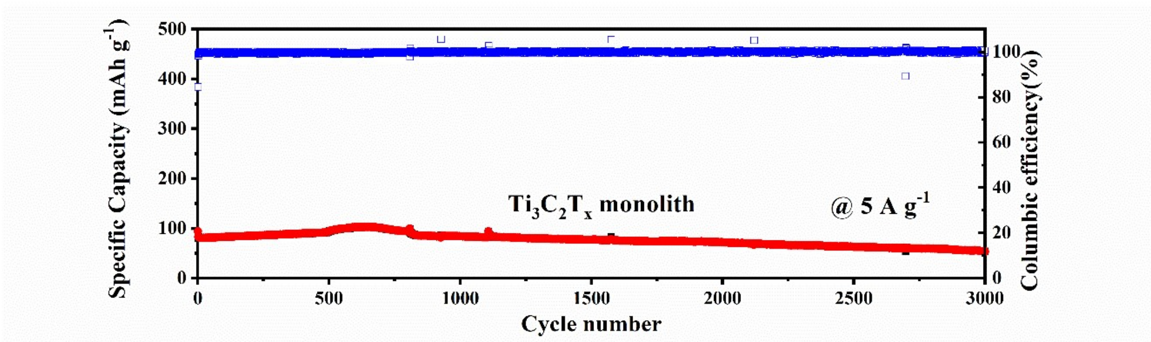

Figure S18 Cycling performance at 5 A g^{-1} of $Ti_3C_2T_x$ monolith

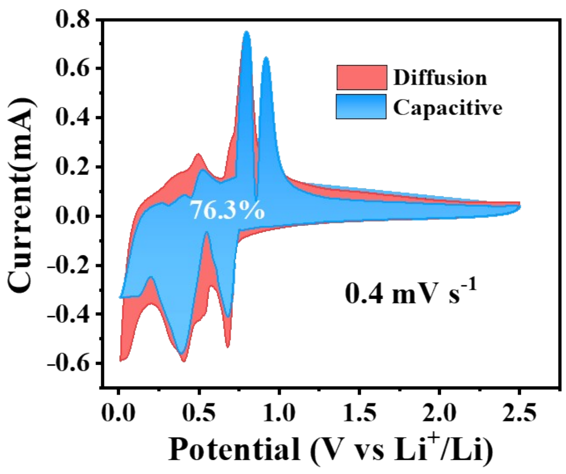

Figure S19 pseudocapacitior contribution at 0.4 mV s^{-1} sweep rate

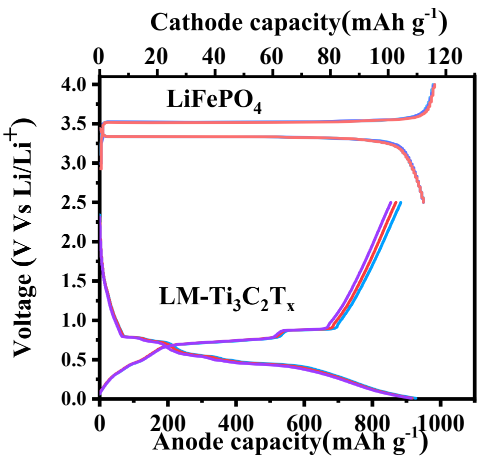

Figure S20 Galvanostatic charge/discharge curves of LM-$Ti_3C_2T_x$ anode and $LiFePO_4$ cathode

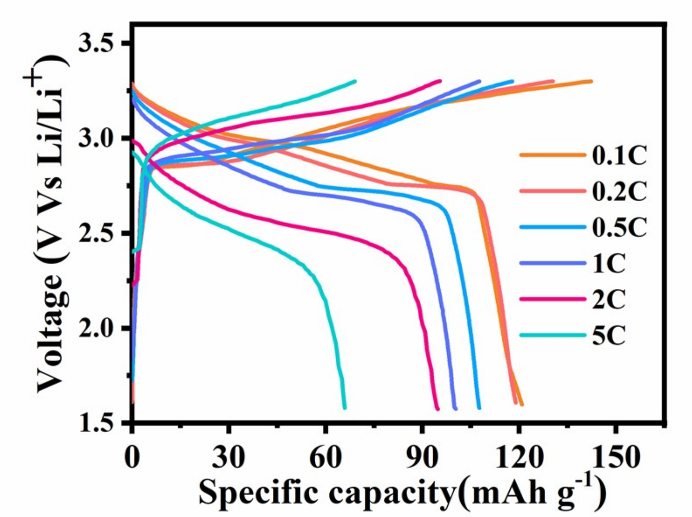

Figure S21 Galvanostatic charge/discharge curves of $LiFePO_4$//LM-$Ti_3C_2T_x$ full cells at different current density (1C=170 mA g^{-1}), demonstrating good rate performance in practical applications.

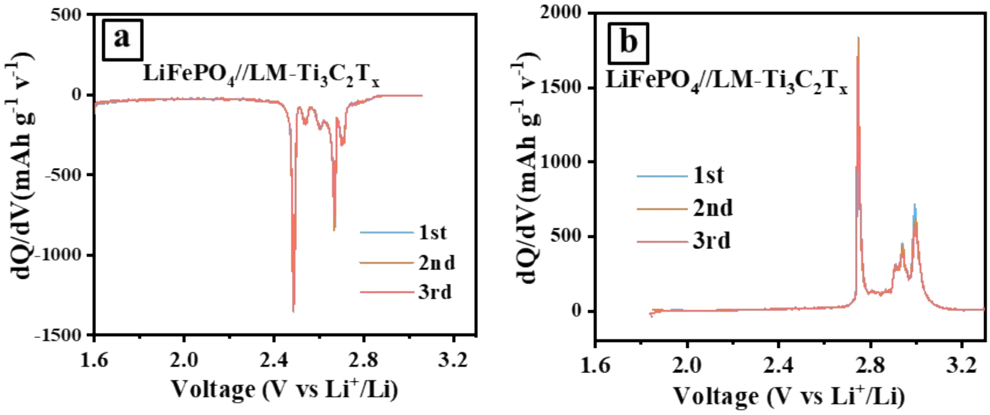

Figure S22 dQ/dv (a) discharge and (b)charge curves of LFP//LM-$Ti_3C_2T_x$ with high magnification

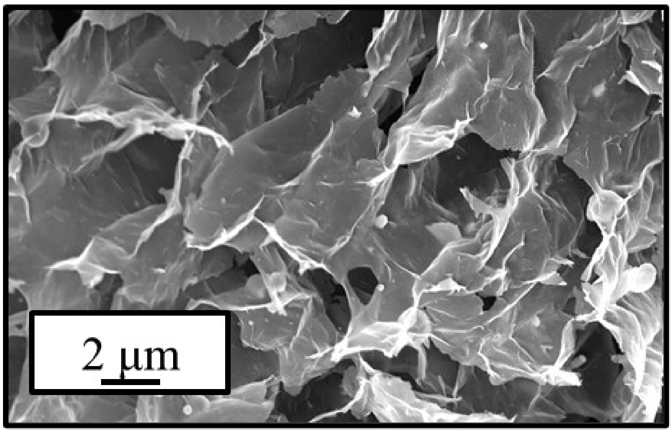

Figure S23 SEM image of LM-$Ti_3C_2T_x$ electrode with a 3D architecture

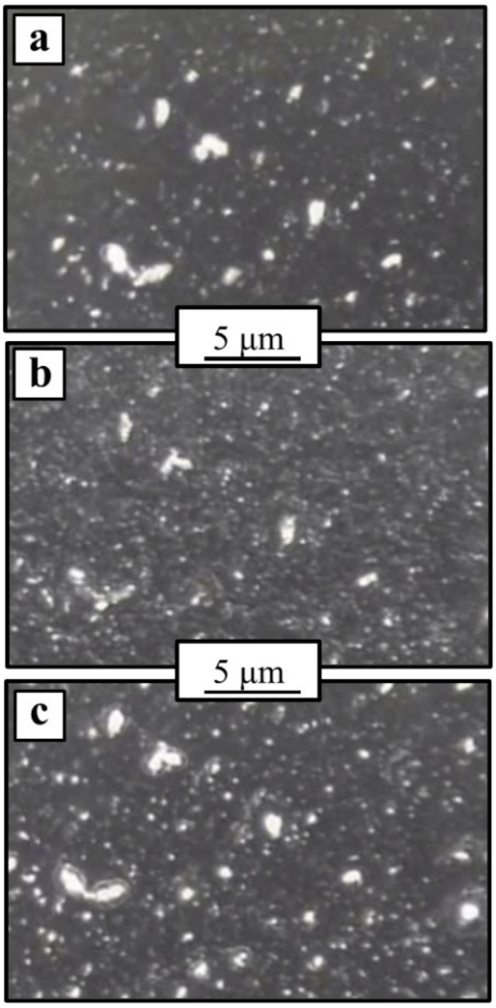

Figure S24 (a) In-situ optical images of LM-$Ti_3C_2T_x$ electrode before cycle, (b) fully alloying and (c) fully de-alloying.

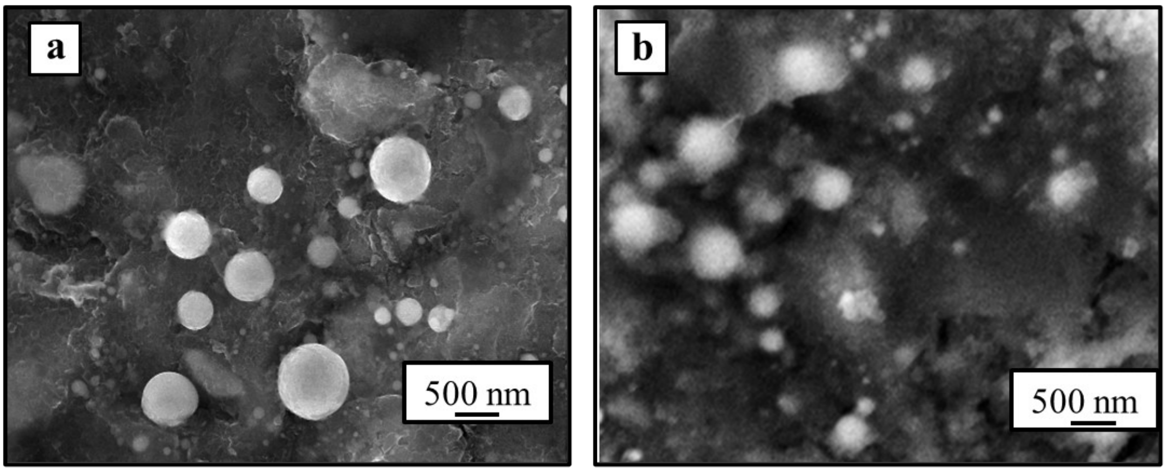

Figure S25 (a) SEM images of LM-$Ti_3C_2T_x$ anode before cycle and (b) SEM images of LM-$Ti_3C_2T_x$ anode after 4500 cycles, which showed a similar spherical morphology compared with initial state. The cyclic process was under 5 A g^{-1} current density.

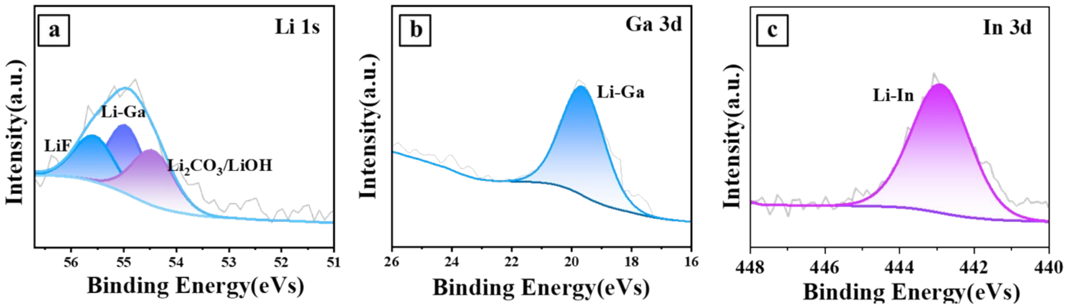

Figure S26 XPS Li 1s, Ga 3d and In 3d spectrum of LM-$Ti_3C_2T_x$ anode after lithiated

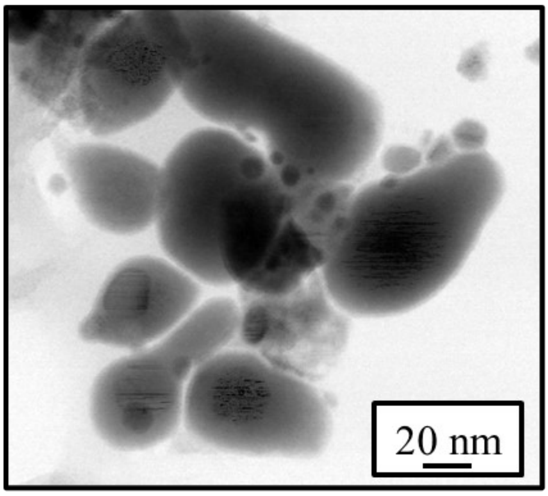

Figure S27 STEM image of the LMNPs after fully alloying, showing a phase separation of Ga and In.

Table S1 Comparison of Ga-based liquid metal performance for LIBs anode

Anode	Capacity	Characteristic	Ref
Ga	~400 mAh g^{-1} at 0.2 C	Under 40°C working conditions	[2]
Ga-In	400 mAh g^{-1} at 5 C; ~400 mAh g^{-1} at 3 C after 500 cycles	Mixed with conductive addiction	[3]
Ga-Sn	493, 419 mAh g^{-1} at 2, 3 A g^{-1}; 400 mAh g^{-1} at 4 A g^{-1} after 4000 cycles	3D Graphene/CNTs as skeleton	[4]
Ga-Sn	603 and 499 mAh g^{-1} at 1 and 2 A/g; 552 mAh g^{-1} at 1 A g^{-1} after 1500 cycles	Hollow MWCNTs nanofibers	[5]

Ga-In-Sn-Zn	404 mAh g^{-1} at 1 A g^{-1}; lower than 400 mAh g^{-1} at 0.5 A g^{-1} after 50 cycles	Utilizing MXene papers as current collectors	[6]
Ga-In	402.7, and 379.6 mAh g^{-1} at 2 and 3 A g^{-1}; 151 mAh g^{-1} at 1 A g^{-1} after 600 cycles	Ultrasonic sieving of gallium-indium alloy particle size	[7]
Ga-In-Sn	350, 270, 246, 234 and 200 mAh g^{-1} at 121, 242, 363 484 and 605 mA g^{-1}; 350.6 mAh g^{-1} after 16 cycles at 60.5 mA g^{-1}	a simple high-speed stirring method	[8]
Ga-In	773, 675, 607, 462, and 350 mAh g^{-1} at 0.1, 0.2, 0.5, 1.0 and2.0 A g^{-1}; 499.8 mAh g^{-1} after 500 cycles at 1.0 A g^{-1}	A tightly PPy wrapped EGaSn structure is formed during the in-situ polymerization synthesis process	[9]
Ga-In	542.8, 479.7, 434.0, 414.1, 387.1, and 380.4 mAh g^{-1} at 0.1, 0.2, 0.5, 1, 2, and 3 A g^{-1}; lower than 200 mAh g^{-1} after 800 cycles at 1.0 A g^{-1}	LMNPs with modified interface	[10]
Ga-In	716, 580, 475, 415, and 351 mAh g^{-1} at 80, 160, 400, 800 and 1.6 A g^{-1}; 397.4 mAh g^{-1} at 1 A g^{-1} after 150 cycles	a simple one-step suction filter method was adopted to load EGaIn NPs on the self-supported CNF/CNT conductive network	[11]
Ga-In	886.5, 647.3, 552.1, and 427.5 mA h g^{-1} at 0.1, 0.5, 1, and 2 A g^{-1}; 300 mAh g^{-1} at 4 A g^{-1} after 700 cycles	EGaIn NPs@PVP core-shell structure	[12]
This work	**489 mAh g^{-1} at 5 A g^{-1}; 409.8 mAh g^{-1} at 5 A g^{-1} after 4500 cycles**	In-situ encapsulation of LM by $Ti_3C_2T_x$-MXene, enable the self-healing ability	

The composition of the LM after full lithiation is relatively simple, only consisting of Li_2Ga and Li_2In. Therefore, the calculation process of the composition contents is based on the following equations (take Li as the example), while the mass of Gallium-indium alloy is normalized.

$$n(\mathrm{Li}) = 2\times(\frac{m(\mathrm{Ga})}{M(\mathrm{Ga})}+\frac{m(\mathrm{In})}{\mathrm{M(In)}}) = 2\times(\frac{0.75g}{69g/mol}+\frac{0.25g}{114g/mol}) = 0.0262\,\mathrm{mol}$$

$$\mathrm{m(Li)} = n(\mathrm{Li})\times\mathrm{M(Li)} = 0.183\,\mathrm{g}$$

$$\omega(\text{Li}) = \frac{m(\text{Li})}{m(\text{Li}) + m(\text{Ga}) + m(\text{In})} = 15.47wt\%$$

Table S2 Composition of Li-Ga-In contents

Elements	Before lithiation contents (wt %)	After lithiation contents (wt %)
Li	0	15.84
Ga	75	63.55
In	25	20.61

References

[1] Z.Y. Zhao, J.W. Han, F.Q. Chen, J. Xiao, Y.F. Zhao, Y.F. Zhang, D.B. Kong, Z. Weng, S.C. Wu and Q.H. Yang, *Adv. Energy. Mater*, **2022**, 12, 2103565.

[2] R. D. Deshpande, J. Li, Y.-T. Cheng and M. W. Verbrugge, *J. Electrochem. Soc*, **2011**, 158, A845-A849.

[3] X. Guo, Y. Ding, L. Xue, L. Zhang, C. Zhang, J. B. Goodenough and G. Yu, *Adv. Funct. Mater*. **2018**, 28. 1804649.

[4] Y. Wu, L. Huang, X. Huang, X. Guo, D. Liu, D. Zheng, X. Zhang, R. Ren, D. Qu and J. Chen, *Energy Environ. Sci.* **2017**, 10, 1854-1861.

[5] J. Zhu, Y. Wu, X. Huang, L. Huang, M. Cao, G. Song, X. Guo, X. Sui, R. Ren and J. Chen, *Nano Energy*. **2019**, 62, 883-889.

[6] C. Wei, H. Fei, Y. Tian, Y. An, G. Zeng, J. Feng and Y. Qian, *Small.* **2019**, 15, e1903214.

[7] C.H. Huang, J.J. Zong, X.D. Wang, Q.P. Cao, D.X. Zhang and J.Z. Jiang, *Materials*, **2021**, 14, 1759.

[8] Y. Qi, C. Shen, Q. Hou, Z. Ren, T. Jin and K. Xie, *J. Energy. Chem*, **2022**, 72, 522-531.

[9] Y. Huang, H. Wang, Y. Jiang and X. Jiang, *Mater. Lett*, **2020**, 276, 128261.

[10] C. Huang, X. Wang, Q. Cao, D. Zhang and J.-Z. Jiang, *ACS Appl. Energy. Mater*, **2021**, 4, 12224-12231.

[11] J. Yu, J. Xia, X. Guan, G. Xiong, H. Zhou, S. Yin, L. Chen, Y. Yang, S. Zhang, Y. Xing and P. Yang, *Electrochimica Acta*, **2022**, 425, 140721.

[12] Y. Liu, Q. Wang, S. Bi, W. Zhang, H. Zhou and X. Jiang, *Nanoscale*, **2020**, 12, 13731-13741.